Optical properties and the optical joint density of states of the misfit-layer compounds $(MS)_{1+x}TS_2$

1994 J. Phys.: Condens. Matter 6 8655

(http://iopscience.iop.org/0953-8984/6/41/027)

J. Phys.: Condens. Matter 6 (1994) 8655–8668. Printed in the UK

Optical properties and the optical joint density of states of the misfit-layer compounds $(MS)_{1+x}TS_2$

Youichi Ohno

Department of Physics, Faculty of General Education, Utsunomiya University, 350 Mine-machi, 321 Utsunomiya, Tochigi, Japan

Received 18 March 1994, in final form 8 July 1994

Abstract. The complex dielectric constant (ε), the absorption coefficient (A), the reflectivity (R), and the optical joint density of states (JDS) of the misfit-layer compounds $(MS)_{1+x}TS_2$ (M = Sn, Pb, Bi, Ce, Sm; T = Ti, Nb) have been derived from reflection electron-energy-loss spectra via Kramers–Kronig analysis. Loss structures arising from interband transitions and a partial plasma resonance have been studied systematically. It is considered that most of the main structures result predominantly from a TS_2 layer. A main contribution from an MS layer causes a loosely varied background as a whole, leading to a decrease in depth of a valley at the optical gap of TS_2. It also gives a high optical JDS at 3–4 eV for the Sn and Pb compounds and at 6–7 eV for the rare-earth compounds. A reasonable interpretation of most experimental results obtained has been made within the rigid-band model in terms of the electronic structure of each layer, although a small deviation from the model must be considered.

1. Introduction

Since 1988, misfit-layer compounds represented by $(MX)_{1+x}TX_2$ ($x = 0.05$–0.25) or roughly represented by MTX_3, have extensively been studied in aspects of crystal growth, crystal structure, electrical and magnetic properties, and electron and x-ray spectroscopy (Wiegers and Meerschaut 1992a, b, Kuypers and van Landuyt 1992). To date about 50 compounds have been synthesized in this family; they are summarized in table 1. The crystals are characterized by alternate stacking of MX and TX_2 layers on an atomic scale, where M is Sn, Pb, Bi, Y, and rare-earth metals, X is chalcogen atoms, and T is transition metals. Most of the experimental results have been discussed within the rigid-band model. Taking the charge transfer from MX to TX_2 layers into account, the electronic structure is regarded approximately as being constructed of the energy band structure of each layer. However, no band calculations have been carried out due to the large unit cell of the incommensurate lattice and there have been few optical studies so far. Recently, Suzuki *et al* (1993) and Hangyo *et al* (1993) have measured infrared reflectance spectra to investigate the electronic structure in the neighbourhood of the Fermi level.

This paper presents the complex dielectric constant (ε), the absorption coefficient (A), the reflectivity (R),and the optical joint density of states (JDS) of MTS_3 (M = Sn, Pb, Bi, Ce and Sm; T = Ti and Nb). The physical quantities have been derived from the reflection electron-energy-loss spectroscopy (REELS) spectra via Kramers–Kronig (KK) analysis. The high-resolution second-derivative REELS spectra measured at the incident energy (E_0) of 100 eV are also presented to discuss single and collective excitation of electrons as well as the electronic structure.

0953-8984/94/418655+14$19.50

Table 1. Misfit-layer compounds $(MX)_{1+x}TX_2$ synthesized to date.

	Sn	Pb	Bi	Y	La	Ce	Pr	Nd	Pm	Sm	Eu	Gd	Tb	Dy	Ho	Er	Tm	Yb	Lu
Ti	S	S	S		S														
			Se																
V		S	S		S	S		S		S		S							
	Se		Se																
Cr				S	S			S				S		S	S	S			
Nb	S	S	S	S	S	S	S	S		S		S	S	S	S	S		S	
	Se	Se	Se																
Ta	S	S	S		S	S	S	S		S		S	S	S		S		S	
			Se																

2. Experiments

Single crystals used in the present experiments were grown from constituent elements by chemical vapour transport reaction in a sealed silica ampoule. Atomically clean surfaces for REELS measurements were prepared by cleaving with adhesive tape in the atmosphere. The REELS measurements were made with a cylindrical-mirror analyser (CMA) equipped with a coaxial-incidence electron gun operated under ultra-high vacuum conditions. The background pressure in operation was of the order of 10^{-8} Pa. To investigate fine loss structures, the high-resolution REELS spectra were measured in second-derivative mode, using a lock-in amplifier. The modulation voltage applied to the incident electron beam was 0.5 eV. The spectra for the KK analysis were measured in pulse-counting mode at $E_0 = 2000$ eV, where dipole selection rules are fulfilled sufficiently. Our instrument and data acquisition and processing systems have been described in a previous paper (Ohno 1987).

The KK analysis was carried out using the data-treatment method previously been exploited for the analysis of MoS_2, one of the layered transition-metal disulphides (Ohno 1989). Since raw REELS spectra are measured on an arbitrary scale, the relations $\mathrm{Re}(1/\varepsilon(0)) = 1/\varepsilon_1(0) = 1/n_\infty^2$ are employed for a semiconductor to derive the energy-loss function, where $\varepsilon(0)$ and $\varepsilon_1(0)$ are the complex dielectric constant and its real part at $E = 0$, respectively, and n_∞ is the long-wavelength limit of the refractive index. Similarly the relation $\mathrm{Re}(1/\varepsilon(0)) = 0$ is employed for a metal. Unfortunately, at present there are no available data for the quantities of the misfit-layer compounds and it is questionable whether the relations are still valid for these compounds, because they are constructed of layers with different dielectric and electrical properties, e.g., an MS layer is semiconducting and a TS_2 layer is metallic. In this study we have used the Bethe f sum rule, although it is not sufficient to derive the absolute energy-loss function. Finally, the present KK analysis allows only qualitative discussion on the optical JDS and optical properties. Nevertheless, it gives valuable information on them at the present time when no optical studies in a wide energy region have been performed.

3. Results and discussion

3.1. Energy band structure of MS and TS_2

3.1.1. β-SnS and PbS. β-SnS crystallizes in the TlI type of structure, constructed of the same double SnS layers as contained in the misfit-layer compounds. The band calculation has been carried out by Tremel and Hoffmann (1987) and Ettema *et al* (1992). The valence bands consist of the S 3s band located around 12 eV below the Fermi level, and Sn 5s band located around 6 eV below the Fermi level, and the upper S 3p band. The Sn 5s band is hybridized with S 3s and 3p states while the S 3p band is hybridized with the Sn 5s and 5p states. The lower conduction band consists of the broad Sn 5p band. The energy gap between the top of the S 3p valence band and the bottom of the Sn 5p conduction band has been estimated by Ettema *et al* (1992) to be about 0.3 eV.

PbS crystallizes in the NaCl type of structure. The band calculation has been carried out by Lin and Kleinman (1966), Herman *et al* (1968), Tung and Cohen (1969), and Kohn *et al* (1973). The valence-band structure has also been studied by the photoemission experiment of McFeely *et al* (1973). According to the results, the band structure is quite similar to that of β-SnS. The valence bands consist of the S 3s band and the Pb 6s band, which are,

respectively, located at 12.8 and 8.4 eV below the Fermi level, and the S 3p band, which is extended to 5 eV from just below the Fermi level with hybridization with Pb 6s and 6p states. Pb 6p states form a broad conduction band, the width being about 10 eV. The energy gap between the top of the S 3p valence band and the bottom of the Pb 6p band is about 0.3 eV.

Both compounds are therefore narrow-gap semiconductors in the bulk state.

3.1.2. CeS and SmS. CeS and SmS crystallize in the NaCl structure like PbS. The band calculation of CeS has been carried out by Soldatov *et al* (1985) and De and Chatterjee (1989). The valence bands consist of the Ce 5p band and the S 3s and 3p bands. The Ce 5p band is localized below the S 3s band, although it is weakly hybridized with S 3s states. The S 3p band, which is located around 3–4 eV below the Fermi level, is hybridized with Ce 5d and 4f states. The conduction bands consist of the Ce 5d and 6s bands and the Fermi level intersects the conduction bands. Thus the compound exhibits metallic properties. According to the augmented-plane-wave (APW) calculation of De and Chatterjee, Ce 4f states form a narrow band with high density of states near the Fermi level, which is immersed in a sea of electrons in the s–d conduction bands. On the other hand, the Korringa–Kohn–Rostocker (KKR) calculation of Soldatov *et al* shows the splitting of Ce 4f states in the energy region between the bottom of the conduction band and the top of the valence band. At present there are no explanations for the difference, although strong correlation seems important for the electrons.

The band calculation of SmS has been carried out by Farberovich (1979) and Lu *et al* (1988). The valence bands consist of the lower S 3s band and the upper S 3p band, which are, respectively, located around 13 and 4 eV below the Fermi level. The energy dispersion of these bands is smaller relative to the same energy bands of β-SnS and PbS. Under normal conditions Sm exists as a divalent ion and the compound exhibits semiconducting properties. Under high pressure, it exhibits metallic properties and Sm exists as a trivalent ion like Sm in $SmNbS_3$. The Sm 4f states are strongly localized. The photoemission experiments of Pollak *et al* (1974), Rowe *et al* (1976), and Chazalviel *et al* (1976) have shown that Sm^{3+} 4f states give multiplet structures (^{5}I, ^{5}F, ^{5}G, and ^{5}D) in the range of 7–11 eV below the Fermi level, whereas Sm^{2+} 4f states give multiplet structures (^{6}H, ^{6}F, and ^{6}P) in the range of 0–3 eV. The conduction bands consist of the Sm 5d and 6s bands, which are largely overlapping. In metallic SmS the Fermi level intersects the conduction bands. The Sm 5d band is split into t_{2g} and e_g bands by the crystal field in the octahedral coordination. Its splitting has been estimated by Batlogg *et al* (1976) to be 2.2 eV.

3.1.3. TiS_2 and NbS_2. TiS_2 crystallizes in the CdI_2 type of structure. The band calculation has been carried out by many workers, e.g., Myron and Freeman (1974), Zunger and Freeman (1977), Bullettt (1978), Umrigar *et al* (1982), and Dijkstra *et al* (1989). The valence bands consist of the S 3s band located around 13 eV below the Fermi level and the S 3p band, which is extended to 5 eV below the Fermi level with strong hybridization with Ti 3d, 4s, 4p states. The lower conduction bands consist of the Ti 3d band and Ti 4s and 4p bands. The Ti 3d band is split into t_{2g} and e_g bands by the crystal field in the octahedral coordination. The energy gap between the top of the S 3p valence band and the bottom of the lowest Ti 3d t_{2g} band is about 0.5 eV, although the reported values are slightly different worker by worker. Thus pure TiS_2 is a narrow-gap semiconductor.

NbS_2 crystallizes in the MoS_2 type of structure in which the metal atoms are surrounded trigonal prismatically by six S atoms. The band calculation has been carried out by Kasowski (1973), Mattheiss (1973), and Doran *et al* (1978). The valence bands consist of the lower S

3s band and the upper S 3p band like TiS_2. The lower conduction bands consist of the Nb 4d band and the Nb 5s and 5p bands, which are strongly hybridized with S 3p states. The Nb 4d band is split into d_{z^2}, $d_{x^2-y^2}$, and d_{xy}, and d_{xz} and d_{yz} bands by the crystal field in the trigonal prismatic coordination. Since the lowest d_{z^2} band is half-filled by one electron per chemical formula, the compound is metallic.

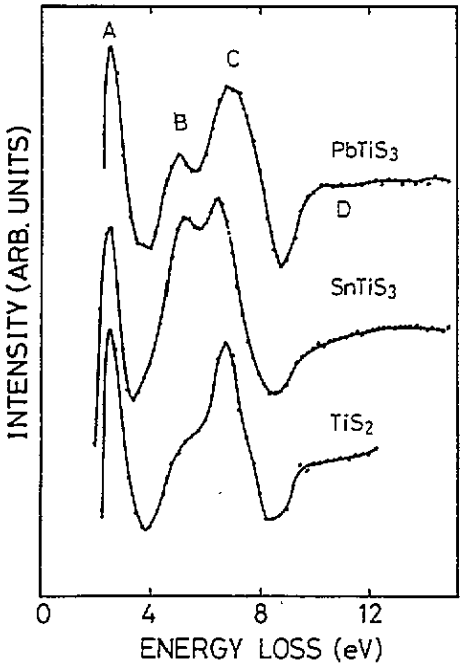

Figure 1. REELS spectra of $PbTiS_3$, $SnTiS_3$, and TiS_2 measured at $E_0 = 100$ eV in second-derivative mode.

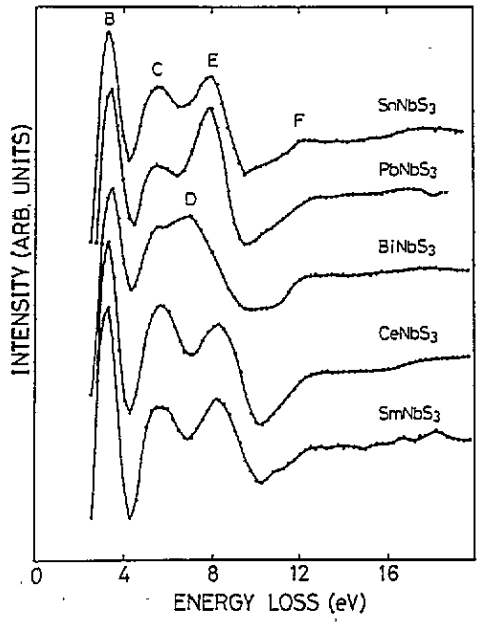

Figure 2. REELS spectra of $MNbS_3$ (M = Sn, Pb, Bi, Ce and Sm) measured at $E_0 = 100$ eV in second-derivative mode.

3.2. Energy loss structures

Figures 1–4 show the REELS spectra of the misfit-layer compounds, which are classified into groups of the same constituent MS and TS_2 layers. It is found from the comparison that the spectra are more similar among the compounds constructed of the same TS_2 layer than those of the same MS layer. Taking the energy band structure into account, we may suggest that the similarity reflects the higher and more undulating densities of states of the energy bands of a TS_2 layer. Although the optical JDSs of SnS and PbS have a maximum at 3–4 eV and the optical JDSs of CeS and metallic SmS give a broad peak at 6–7 eV, their contribution has a minor effect on the main structures as discussed later. Interband transitions within an MS layer seem to contribute to a loosely varied background in the energy region of our interest.

3.2.1. The Ti compounds. Figure 1 shows the REELS spectra of $SnTiS_3$, $PbTiS_3$, and TiS_2. We find a sharp peak at 2.5 eV at which the optical JDS shows a minimum. The peak thus arises from a partial plasma resonance, which occurs when interband transitions involving a subgroup of the JDS are exhausted. According to the band calculation of Dijkstra *et al*

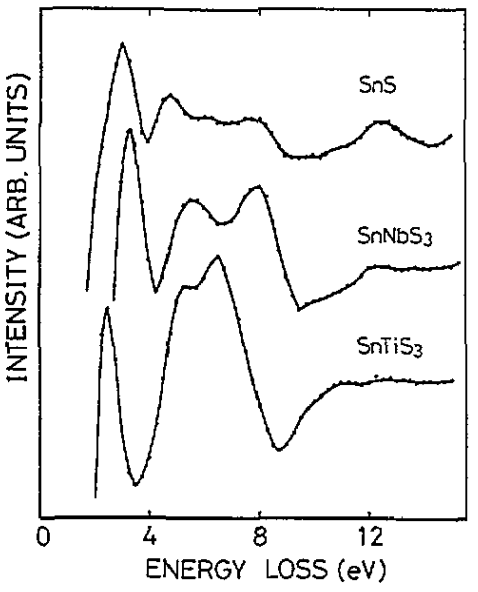

Figure 3. REELS spectra of $SnTiS_3$, $SnNbS_3$, and SnS measured at $E_0 = 100$ eV in second-derivative mode.

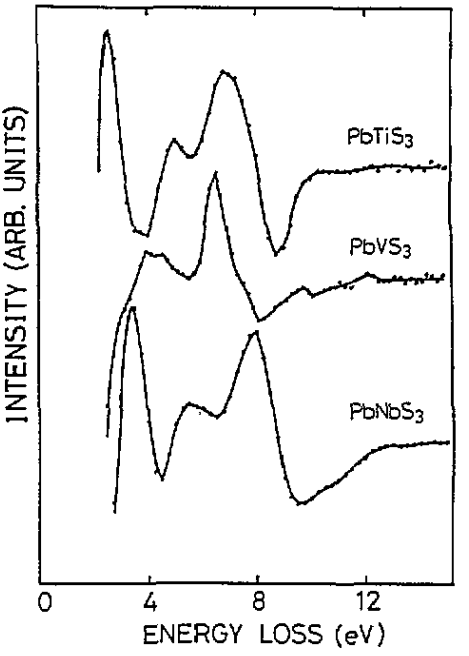

Figure 4. REELS spectra of $PbTS_3$ (T = Ti, V and Nb) measured at $E_0 = 100$ eV in second-derivative mode.

(1989), the widths of the Ti 3d t_{2g} and e_g bands are 1.61 and 1.50 eV, respectively. Many experimental and theoretical results (Chen *et al* 1980, Doni and Girlanda 1986) show a d/p band gap less than 0.5 eV and a crystal-field splitting of the t_{2g} and e_g bands of about 2 eV. From these facts, we may suggest that an optical gap is created at 2.5 eV from the exhaustion of interband transitions from the high density of states in the top region of the S 3p valence band to unoccupied Ti 3d t_{2g} states. A loss peak at 5.0 eV, which appears at the maximum in the optical JDS, may be assigned to interband transitions from the S 3p valence band to the Ti 3d e_g band within a TiS_2 layer, although there is a non-negligible contribution from an SnS or a PbS layer. A loss peak around 6.8 eV shifts to higher energy with incident energy until it reaches 7.7 and 8.0 eV at $E_0 = 2000$ eV for $SnTiS_3$ and $PbTiS_3$, respectively. Since a large dip occurs in this energy region in the optical JDS, it is attributed to collective excitation of electrons. This partial plasma resonance arises from the exhaustion of interband transitions to the d conduction band. Finally, we may assign a broad structure around 12 eV to interband transitions from the S 3p valence band to the s–p conduction band. The main features are summarized in table 2. The ω_L peaks show the partial plasma resonance whereas the ω_T peaks show interband transitions.

3.2.2. The Nb compounds. Figure 2 shows the REELS spectra of $MNbS_3$ (M = Sn, Pb, Bi, Ce and Sm). The main features are tabulated in table 3 together with those of NbS_2, which have been deduced from the transmission EELS spectrum by Bell and Liang (1976) and Manzuke *et al* (1986). The loss peak A at 1.0 eV is not found in our spectra due to the influence of a large elastic peak. For NbS_2 the energy gap between the Nb 4d conduction band and the higher-energy s–p conduction band is responsible for a large dip of the optical JDS around 8 eV. The loss peak E is assigned to a partial plasma resonance, i.e., the collective excitation of nine or eight electrons depending on the number of unoccupied d states. Such

Table 2. The energies in electronvolts of the loss peaks of $SnTiS_3$, $PbTiS_3$, and TiS_2 and their assignments. ω_L represents the frequency of a partial plasma resonance and ω_T represents the root mean square of transition frequencies weighted by oscillator strength.

Notation	$SnTiS_3$	$PbTiS_3$	TiS_2	Assignment
A	2.5	2.5	2.5	ω_L
B	5.2	5.0	5.0	ω_T
C	6.4	6.9	6.8	ω_L
D	11.8	11.0	12.0	ω_T

Table 3. The energies in electronvolts of the loss peaks of $MNbS_3$ (M = Sn, Pb, Bi, Ce, and Sm) and NbS_2 and their assignments. ω_L represents the frequency of a partial plasma resonance and ω_T represents the root mean square of transition frequencies weighted by oscillator strength.

Notation	$SnNbS_3$	$PbNbS_3$	$BiNbS_3$	$CeNbS_3$	$SmNbS_3$	NbS_2	Assignment
A						1.0[a]	ω_L
B	3.5	3.4	3.5	3.3	3.3	3.5	ω_L
C	5.7	5.7	5.5	5.7	5.5	5.4	ω_T
D			7.0				ω_T
E	8.0	8.0	8.0	8.3	8.2	8.5	ω_L
F	12.9	12.5	12.5	12.5	12.5		ω_T

[a] Bell and Liang (1976).

an assignment has already been made by Bell and Liang (1976). We may connect the loss peak B to a small dip in the optical JDS, which arises from an energy gap between the d_{z^2} and the upper d bands. It is therefore attributed to a partial plasma resonance due to the exhaustion of interband transitions to unoccupied d_{z^2} states. On the other hand, the loss peaks C, D and F are assigned to interband transitions from the S 3p valence band to the upper d bands and to the s–p conduction bands because the optical JDS shows a large intensity at the peak energies.

3.3. Kramers–Kronig analysis

In the previous paper (Ohno 1989) the present author has shown that the KK analysis for the REELS spectra measured with a CMA at incident energies of more than 500 eV is valid to derive optical properties and the optical JDS in a wide energy region by removing the background arising from multiple scattering and secondary-electron emission and the surface effects by appropriate methods. This technique has firstly been applied to the REELS spectrum of MoS_2. The resulting spectra are in good agreement with the optical spectra of Liang (1973) and those derived from the energy-loss function parallel to the layers, which is deduced from the transmission EELS spectrum (Ohno 1989, Bell and Liang 1976, Zeppenfeld 1970). Similar attempts have since been made by Yubero *et al* (1990, 1991), Yubero and Touggard (1992) and Ingram *et al* (1990a, b). They have applied it to the REELS spectra of Zr, ZrO_2, Al, Cu, Ag and Au. Although they have used a different type of analyser, i.e., a hemispherical analyser, they have drawn the same conclusions.

Figure 5 shows the KK results for TiS_2. On comparing the resulting R spectrum with the optical spectra of Greenaway and Nitsche (1965) and Hughes and Liang (1977), we find that there is a good agreement between them. In spite of the disappearance of fine structures due to a lower energy resolution, it is clear that the KK analysis is practical for the compound. The same application has therefore been made for the REELS spectra of seven of the misfit-layer compounds and SnS. Figure 6 shows the results for SnS. In comparison

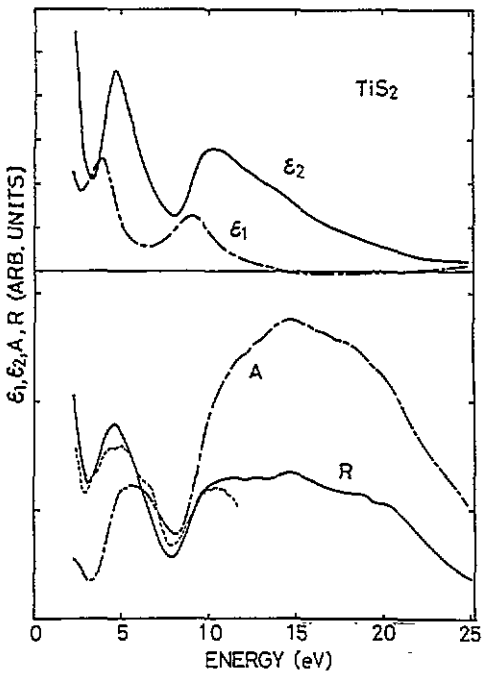

Figure 5. The real and imaginary parts of the dielectric constant, the reflectivity R, and the absorption coefficient A of TiS_2, which have been derived from the REELS spectrum at $E_0 = 2000$ eV via the KK analysis. A broken line shows the R spectrum obtained by Greenaway and Nitsche (1965).

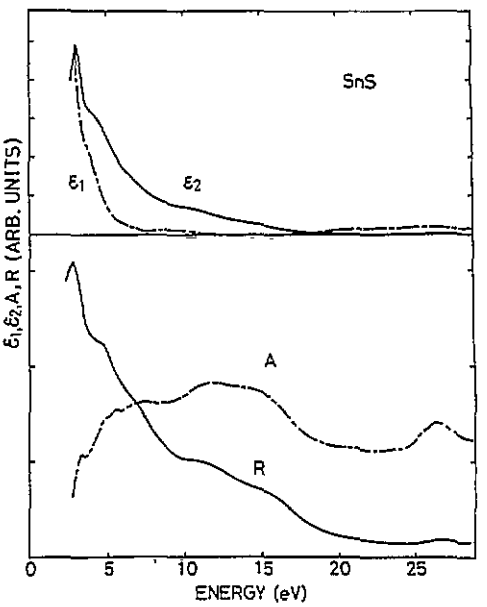

Figure 6. The real and imaginary parts of the dielectric constant, the reflectivity R, and the absorption coefficient A of SnS, which have been derived from the REELS spectrum at $E_0 = 2000$ eV via the KK analysis.

with the KK results for the transmission EELS spectrum (Eymard and Otto 1977), ε_1, the real part of the complex dielectric constant, becomes positive in the range of 5–10 eV. A similar result has previously been reported for Zr by Yubero *et al* (1990), who have indicated that this is caused by a surface effect. In a similar way it is considered that the positive values are caused by imperfect removal of a surface loss function. In spite of the disagreement, overall structures are in coincidence between them. The KK analysis is thus still valid for SnS. We may also suggest that ε_2, the imaginary part of the complex dielectric constant, decreases monotonically from a maximum value at 3 eV as energy increases.

3.3.1. Optical properties. Figure 7 shows the KK results for the misfit-layer compounds. In the Ti compounds as in TiS_2 ε_2 has a maximum at 4.8 eV, which arises primarily from interband transitions from the S 3p valence band to the Ti 3d e_g band. Interband transitions to the t_{2g} band, on the other hand, give a peak around 2 eV for TiS_2. In our spectra, unfortunately, any structures below 2 eV are omitted to avoid the confusion due to artificial structures by an elastic peak. In the measurements the half width at half maximum of the elastic peak is 0.4 eV, the first minimum appears at 1.5 eV above the elastic peak, and the intensity at 2.0 eV above the elastic peak is about three times larger than the intensity at 2.0 eV below the peak. Then we may assume that the influence is negligible at energy greater than 2 eV. In practice the resulting optical spectra for MoS_2 show a good agreement with those of the optical experiments in the same energy region (Ohno 1989). At the low-energy limit in figure 5, a sharp rise is found, indicating the existence of a peak on the

lower energy side. Such a rise is not observed for $SnTiS_3$ and $PbTiS_3$. The disappearance is not well explained within the rigid-band model because the structure arises from interband transitions from the S 3p valence states to the empty 3d t_{2g} states at the Γ point, which remain almost unchanged against a small Fermi-energy shift, which is expected by charge transfer from MS layers. It appears therefore that the electronic structure near the Fermi level varies from the bulk compound and the rigid-band model is broken in a rigorous sense. A better explanation is given by the reduced energy dispersion upon insertion of MS layers. If the highest S 3p level and/or the Ti 3d t_{2g} band became narrower, the peak would shift to lower energies. This means an increase in two dimensionality of a TiS_2 layer, which is partially supported by more prominent anisotropy in electric conductivities parallel and perpendicular to the layers.

The resulting R and A spectra show a minimum around 8 eV, which is caused by the exhaustion of interband transitions from the S 3p valence band to the Ti 3d e_g band and the beginning of interband transitions to the higher s–p conduction bands. The optical gap is therefore related to the plasma loss peak around 6.8 eV, which shifts to 8 eV at $E_0 = 2000$ eV. For $PbTiS_3$ fine structures are observed in the range of 20–23 eV. These are caused by excitation of Pb 5d core electrons. For $SnTiS_3$ fine structures are found around 26 eV; these are caused by Sn 4d excitation. According to the experimental and theoretical studies of Kohn *et al* (1973), ε_2 for PbS has a maximum at 3 eV and then monotonically decreases as the energy increases to 8 eV. The contribution from a PbS layer therefore gives a loosely varied background in the range of 3–8 eV as for SnS.

In comparison with the Ti compounds, the Nb compounds give an A spectrum that has an additional structure as 3–3.5 eV. This structure originates from interband transitions from the S 3p valence band to the incompletely filled d_{z^2} band. The intensity decreases from the Sn, Pb and Bi compounds to the rare-earth compounds. Since for the rare-earth compounds more intensive charge transfer or a smaller number of unoccupied d_{z^2} states has been confirmed by electrical measurements (Wiegers *et al* 1990, 1991) and infrared reflectance studies (Suzuki *et al* 1993, Hangyo *et al* 1993), the reduced intensity may be attributed to the larger occupation of the half-filled d_{z^2} band with transferred electrons. ε_2 and R for the rare-earth compounds exhibit a more prominent dip around 3.8 eV and an additional structure around 6 eV. Since the R spectra of CeS (Schoenes 1984) and metallic SmS (Batlogg *et al* 1976) have a large dip around 3 eV, followed by a broad peak centred at 6–8 eV, the contribution from the MS layers would enlarge a dip around 3.8 eV. They have also shown that the broad peak is caused by interband transitions from the S 3p valence band to the 5d–6s conduction band of the rare-earth elements. The additional structure around 6 eV may therefore be assigned to the interband transition from the S 3p valence band to the 5d–6s conduction bands. Taking the energy band structure and the valence of Sm in $SmNbS_3$ into account, we may expect that Sm 4f→5d transitions give multiplet structures in the range of 8–15 eV. However, such structures are not observed clearly. The same result has been obtained for CeS by Schoenes (1984), who has found that the Ce 4f→5d transitions are extremely weak, so only a small perturbation happens in the optical conductivity. Thus we may conclude that the transition-matrix elements of the 4f → 5d transitions are small. Similarly the S 3p → Ce 4f transitions are ignored, possibly because of a small overlap of the wavefunctions owing to the spatial and energetic localization of the 4f states. A large contribution from the SnS and PbS layers exists around 3–4 eV as discussed above.

3.3.2. Optical joint density of states. The optical JDSs $J(E) \propto E\varepsilon_2(E)$ of the misfit-layer compounds have been deduced by KK analysis. The results are shown in figures 8 and 9. It

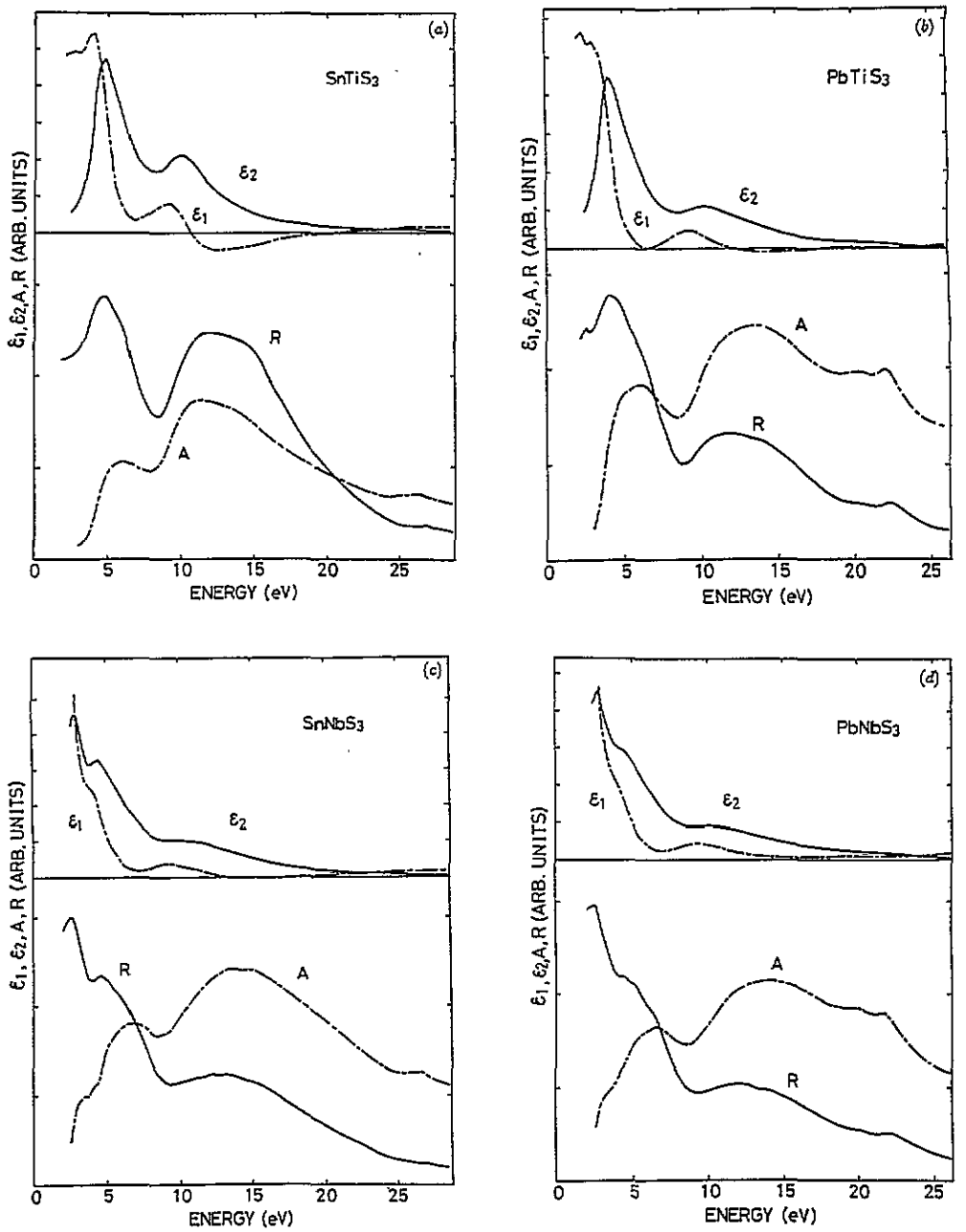

Figure 7. The real and imaginary parts of the dielectric constant, the reflectivity R, and the absorption coefficient A of the misfit-layer compounds, which have been derived from the REELS spectra at $E_0 = 2000$ eV via the KK analysis: (a) $SnTiS_3$; (b) $PbTiS_3$; (c) $SnNbS_3$; (d) $PbNbS_3$; (e) $BiNbS_3$; (f) $CeNbS_3$; and (g) $SmNbS_3$.

is found from figure 8 that the optical JDSs of the Ti compounds consist of two parts, which are separated by a large dip around 8 eV. The high optical JDS around 5 eV arises from the S 3p valence band and the Ti 3d conduction band although there is a contribution from

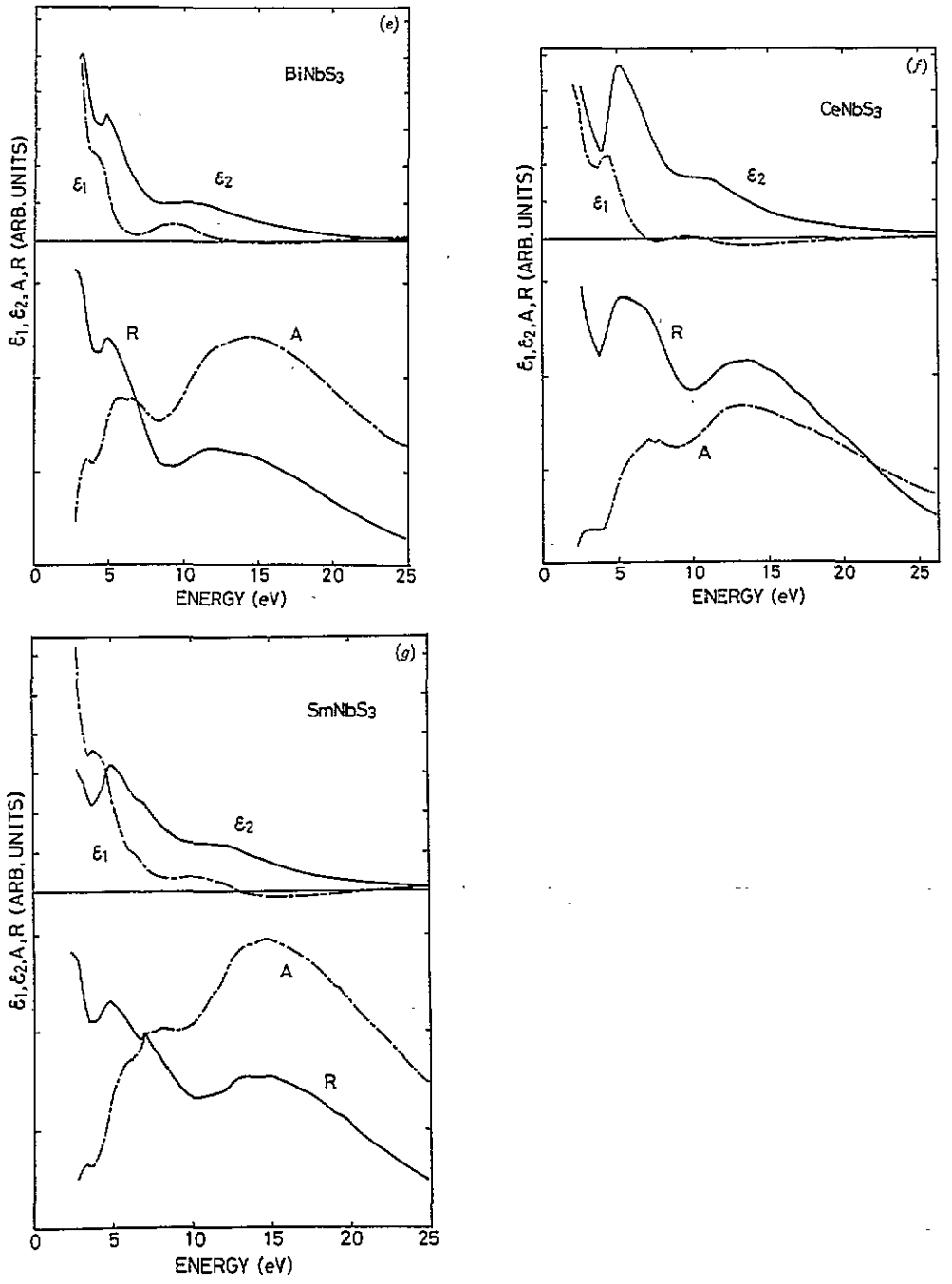

Figure 7. (Continued)

the SnS or PbS layers. The high optical JDS around 10 eV arises primarily from the S 3p valence band and the s–p conduction band within a TiS_2 layer and a shoulder around 14 eV may be attributed to interband transitions from the S 3s band. The optical JDSs of $SnNbS_3$

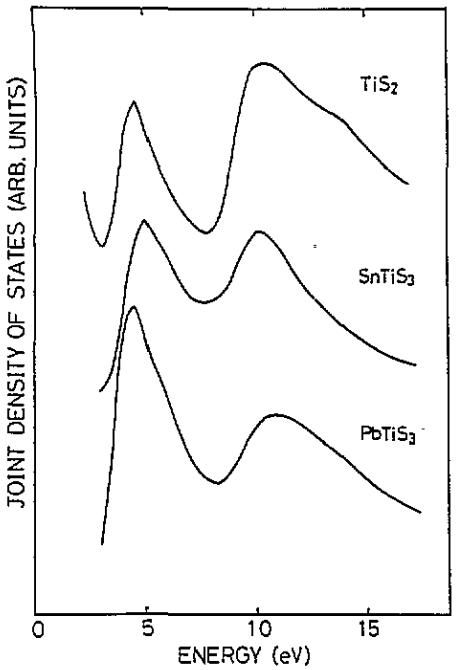

Figure 8. The optical JDSs of $PbTiS_3$, $SnTiS_3$, and TiS_2, which have been derived from the REELS spectra at $E_0 = 2000$ eV via KK analysis.

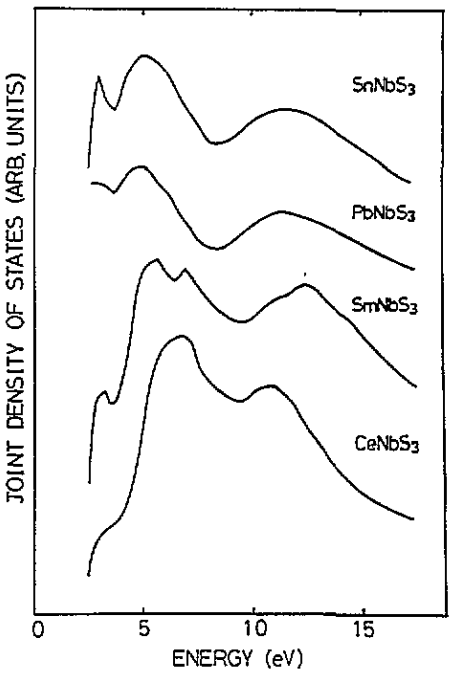

Figure 9. The optical JDSs of $MNbS_3$ (M = Sn, Pb, Ce and Sm), which have been derived from the REELS spectra at $E_0 = 2000$ eV via KK analysis.

and $PbNbS_3$ are different from those of $CeNbS_3$ and $SmNbS_3$. The former is more similar to the optical JDS of $NbSe_2$, akin to NbS_2 (Bell and Liang 1976), possibly due to a weaker interlayer interaction and a smaller contribution from the MS layer. A dip around 8 eV is caused by the small JDS resulting from the energy gap between the d conduction band and the higher-energy s–p conduction band within an NbS_2 layer. A peak or a shoulder at 3.1 eV arises from the high JDS of the S 3p valence band and unoccupied d_{z^2} states and the intensity is reduced by intensive charge transfer for the rare-earth compounds. For $SnNbS_3$ and $PbNbS_3$ it is increased by a large contribution from SnS and PbS layers although charge transfer would exist as in the rare-earth compounds. Finally, the optical JDSs of the rare-earth compounds have additional structures around 6.5 eV. These are caused by the high JDS within the MS (M = Ce and Sm) layers, which arises from the S 3p valence band and the rare-earth-metal 5d–6s conduction band. It is difficult to obtain information on the Ce 4f and Sm 4f states, possibly due to small transition-matrix elements. Thus the JDS is modified strongly in the optical JDS by the matrix-element effect.

4. Conclusions

Some physical quantities such as ε, A, R, and the optical JDS have been derived from the REELS spectra via the KK analysis. Most of the results obtained are well interpreted in terms of the electronic structure of each constituent layer within the rigid-band model. Since the energy band structure of the TS_2 layer is more undulating than that of the MS layer and the density of states is higher except for the localized 4f states of the rare-earth elements, the

main structures are derived dominantly from the TS_2 layer. The transition-matrix elements of the 4f states seem small. The contribution from the MS layer thus has a minor effect on the structures, although it affects a loosely varied background. We have also indicated the breakdown of the rigid-band model. For $SnTiS_3$ and $PbTiS_3$ we present experimental evidence of the variations in electronic structure in the neighbourhood of the Fermi level. A sharp rise at the lower energy limit disappears for the misfit-layer compounds.

The energy-loss structures have been discussed, taking the dielectric constant and the optical JDS into account. The peaks around 2.5 eV and 6.8 eV of the Ti compounds and the peaks around 3.5 eV and 8.0 eV of the Nb compounds arise from the partial plasma resonance, which occurs when interband transitions involving a subgroup of the JDS are exhausted. They are connected to the minima in the *R* and *A* spectra. The loss peak around 5 eV of the Ti compounds and the peak around 5.5 eV of the Nb compounds correspond to the maximum of the optical JDS. They are therefore assigned to the excitation of single electrons within a TS_2 layer. Strong interband transitions within the SnS and PbS layers occur in the range of 3–4 eV while strong interband transitions within the CeS and the metallic SmS layers are present in the range of 5–7 eV. The latter transitions arise from the S 3p valence band to the rare-earth-metal 5d–6s conduction band.

References

Batlogg B, Kaldis E, Schlegel A and Wachter P 1976 *Phys. Rev.* B **14** 5503

Bell M G and Liang W Y 1976 *Adv. Phys.* **25** 53

Bullett D W 1978 *J. Phys. C: Solid State Phys.* **11** 4501

Chazalviel J-N, Campagna M, Wertheim G K and Schmidt P H 1976 *Phys. Rev.* B **14** 4586

Chen C H, Fabian W, Brown F C, Woo K C, Davies B, DeLong B and Thompson A H 1980 *Phys. Rev.* B **21** 615

De S K and Chatterjee S 1989 *Phys. Rev.* B **40** 12304

Dijkstra J, van Bruggen C F and Haas C 1989 *J. Phys.: Condens. Matter* **1** 4297

Doni E and Girlanda R 1986 *Electronic Structure and Electronic Transitions in Layered Materials* ed V Grasso (Tokyo: Reidel) p 1

Doran N J, Ricco B, Titterington D J and Wexler G 1978 *J. Phys. C: Solid State Phys.* **11** 685

Ettema A R H F, de Groot R A, Haas C and turner T S 1992 *Phys. Rev.* B **46** 7363

Eymard R and Otto A 1977 *Phys. Rev.* B **16** 1616

Farberovich O V 1979 *Sov. Phys.–Solid State* **21** 1982

Greenaway D L and Nitsche R 1965 *J. Phys. Chem. Solids* **26** 1445

Hangyo M, Nishio T, Nakashima S, Ohno Y, Terashima T and Kojima N 1993 *Japan. J. Appl. Phys. Suppl.* **32–3** 581

Herman F, Kortum R L, Outenburger I B and Van Dyke J P 1968 *J. Physique Coll.* **29** C4 62

Hughes H P and Liang W Y 1977 *J. Phys. C: Solid State Phys.* **10** 1079

Ingram J C, Nebesny K W and Pemberton J E 1990a *Appl. Surf. Sci.* **44** 279

—— 1990b *Appl. Surf. Sci.* **44** 293

Kasowski R V 1973 *Phys. Rev. Lett.* **30** 1175

Kohn S E, Yu P Y, Petroff Y, Shen Y R, Tsang Y and Cohen M L 1973 *Phys. Rev.* B **8** 1477

Kuypers S and van Landuyt J 1992 *Mater. Sci. Forum* **100 & 101** 223

Liang W Y 1973 *J. Phys. C: Solid State Phys.* **4** L378

Lin P J and Kleinman L 1966 *Phys. Rev.* **142** 478

Lu Z W, Singh D J and Krakaur H 1988 *Phys. Rev.* B **37** 10045

Manzuke R, Fink J and Crecelius G 1986 *Electronic Structure and Electronic Transitions in Layered Materials* ed V Grasso (Tokyo: Reidel) p 480

Mattheiss L F 1973 *Phys. Rev.* B **8** 3719

McFeely F R, Kawalczyk S, Ley L, Pollak R A and Shirley D A 1973 *Phys. Rev.* B **7** 5228

Myron H W and Freeman A J 1974 *Phys. Rev.* B **9** 481

Ohno Y 1987 *Phys. Rev.* B **36** 7500

—— 1989 *Phys. Rev.* B **39** 8209

Pollack R A, Holtzberg F, Freeouf J L and Eastman D E 1974 *Phys. Rev. Lett.* **33** 820

Rowe J E, Campagna M, Christman S B and Bucher E 1976 *Phys. Rev. Lett.* **36** 148
Schoenes J 1984 *NATO ASI Series B* vol 117, p 237
Soldatov A V, Gusatinskii A N and Al'perovich G I 1985 *Sov. Phys.–Solid State* **27** 2061
Suzuki K, Kondo T, Enoki T and Tajima H 1993 private communication
Tremel W and Hoffmann R 1987 *Inorg. Chem.* **26** 118
Tung Y W and Cohen M L 1969 *Phys. Rev.* **180** 823
Umrigar C, Ellis D E, Wang D, Krakauer H and Posternak M 1982 *Phys. Rev.* B **26** 4935
Wiegers G A and Meerschaut A 1992a *Mater. Sci. Forum* **100 & 101** 101
—— 1992b *J. Alloys Compounds* **178** 351
Wiegers G A, Meetsma A, Haange R J and De Boer J L 1990 *J. Solid State Chem.* **89** 328
—— 1991 *J. Less-Common Met.* **168** 347
Yubero F, Sanz J M, Elizalde E and Galan L 1990 *Surf. Sci.* **237** 173
—— 1991 *Surf. Sci.* **251/252** 296
Yubero F and Touggard S 1992 *Phys. Rev.* B **46** 2486
Zeppenfeld K 1970 *Opt. Commun.* **1** 377
Zunger A and Freeman A J 1977 *Phys. Rev.* B **16** 906